PROCEEDINGS OF SPIE

SPIEDigitalLibrary.org/conference-proceedings-of-spie

SF-FDTD analysis of a predictive physical model for parallel aligned liquid crystal devices

Andrés Márquez
Jorge Francés
Francisco J. Martínez
Sergi Gallego
Mariela L. Álvarez
Eva M. Calzado
Inmaculada Pascual
Augusto Beléndez

SPIE.

SF-FDTD analysis of a predictive physical model for parallel aligned liquid crystal devices

Andrés Márquez[1,2], Jorge Francés[1,2], Francisco J. Martínez[1,2], Sergi Gallego[1,2], Mariela L. Alvarez[1,2], Eva M. Calzado[1,2], Inmaculada Pascual[2,3], Augusto Beléndez[1,2]

[1]Dept. de Física, Ing. de Sistemas y T. Señal, Univ. de Alicante, Ap. 99, E-03080, Alicante, Spain
[2]I.U. Física Aplicada a las Ciencias y las Tecnologías U. de Alicante, Ap. 99, E-03080, Alicante, Spain
[3]Dept. de Óptica, Farmacología y Anatomía, Univ. de Alicante, Ap. 99, E-03080, Alicante, Spain

ABSTRACT

Recently we demonstrated a novel and simplified model enabling to calculate the voltage dependent retardance provided by parallel aligned liquid crystal devices (PA-LCoS) for a very wide range of incidence angles and any wavelength in the visible. To our knowledge it represents the most simplified approach still showing predictive capability. Deeper insight into the physics behind the simplified model is necessary to understand if the parameters in the model are physically meaningful. Since the PA-LCoS is a black-box where we do not have information about the physical parameters of the device, we cannot perform this kind of analysis using the experimental retardance measurements. In this work we develop realistic simulations for the non-linear tilt of the liquid crystal director across the thickness of the liquid crystal layer in the PA devices. We consider these profiles to have a sine-like shape, which is a good approximation for typical ranges of applied voltage in commercial PA-LCoS microdisplays. For these simulations we develop a rigorous method based on the split-field finite difference time domain (SF-FDTD) technique which provides realistic retardance values. These values are used as the experimental measurements to which the simplified model is fitted. From this analysis we learn that the simplified model is very robust, providing unambiguous solutions when fitting its parameters. We also learn that two of the parameters in the model are physically meaningful, proving a useful reverse-engineering approach, with predictive capability, to probe into internal characteristics of the PA-LCoS device.

Keywords: Liquid-crystal devices, Parallel-aligned, Birefringence, Spatial light modulators, Displays, Finite-Difference Time-Domain, Split-Field.

1. INTRODUCTION

Parallel-aligned liquid crystal on silicon microdisplays (PA-LCoS)[1][2] are widely used as SLMs in a wide range of applications[3][4]. They enable phase-only modulation of light wavefronts without coupled amplitude modulation, and with millions of addressable pixels. They can be thought as variable linear retarders whose linear retardance is tuned by the applied voltage, and as such they are also interesting devices for spatial modulation of the state of polarization (SOP) of the light wavefront[5]. They can also be used for amplitude modulation[6]. We have also tested their validity for binary intensity and for hybrid ternary modulation, which are interesting modulation regimes in holographic memories[7]. Proper characterization of their linear retardance ensures optimal performance in applications. We proposed time-averaged Stokes polarimetry[5] as an advanced technique which enables robust linear retardance characterization in the presence of flicker, which is a typical degradation phenomenom found in most of LCoS devices[8][9][10].

We recently proposed[11] a reverse-engineering model with predictive capability, based on only three parameters: two off-state (non-voltage dependent), and one on-state (voltage-dependent). To our knowledge, it represents the most simplified approach still showing predictive capability. From a limited amount of measurements, the three parameters in the model are fitted, and then the model is able to provide the voltage dependent retardance for a very wide range of incidence angles and any wavelength in the visible. We demonstrated the good agreement between theoretical and experimental results with errors smaller than 5%. Since in general, when using commercial PA-LCoS devices manufacturers do not give the values of the construction parameters of the device and the liquid crystal material, in the present work we implement a computational simulation of a virtual PA-LC. For the tilt angle profile we consider a sine-like analytical approximation to the realistic non-homogeneous voltage dependent tilt angle profiles[12][13]. Calculation of

Optics and Photonics for Information Processing XI, edited by Khan M. Iftekharuddin, Abdul A. S. Awwal, Mireya García Vázquez, Andrés Marquez, Víctor Diaz-Ramirez, Proc. of SPIE Vol. 10395, 1039509 · © 2017 SPIE · CCC code: 0277-786X/17/$18 · doi: 10.1117/12.2273924

the retardance for this virtual PA-LC cell is accomplished by using the split-field finite-difference time-domain (SF-FDTD) method[14][15][16], which provides rigorous results for the Maxwell equations together with an efficient use of the computing resources. The sine-like profile is an analytic approximation to the realistic tilt angle profile, which is easier to apply and whose accuracy is good enough as long as the applied voltage is not very large. Within the sine-like approximation we find that one of the two off-state parameters, the so-called optical path difference OPD, and the on-state parameter, the equivalent tilt angle, agree very well with the physical values assigned to the construction parameters for the virtual PA-LC cell. Therefore the reverse-engineering model is actually a semi-physical model able to probe into some of the internal properties of PA-LC devices. This is an added value to the simplified model. In the next Section we introduce the basics of the simplified model together with the details of the construction of the virtual PA-LC cell. In Section 3 we show the results obtained when the model is used to fit the SF-FDTD calculated retardances. Eventually, the main conclusions are given in Section 4.

2. REVERSE-ENGINEERING MODEL AND VIRTUAL PA-LC CELL

2.1 Simplified model

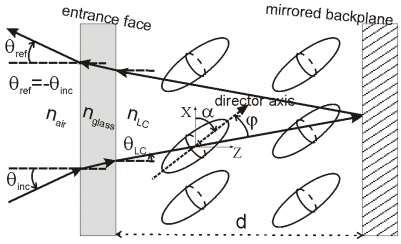

Figure 1. Diagram for the PA-LC cell considered in the model proposed.

We present the basic details of the reverse-engineering simplified model. Further details are available in the previous papers where the model was proposed[11]. Actually, its validity was demonstrated against experimental measurements from a commercial reflective PA-LCoS device. In Fig. 1 we show its general diagram for a reflective cell with a cell gap d. Incidence plane and LC director are along the XZ plane. LC molecules have their director axis (optical axis) aligned at an angle φ with respect to the traversing light beam direction. θ_{LC} is the refraction angle in the LC medium. The director axis tilts an angle α with respect to the entrance face as a function of the applied voltage V. This is the only voltage dependent magnitude, i.e. $\alpha(V)$. At the backplane the light beam is reflected and a second passage is produced across the LC layer whose effect is equivalent to a forward propagation at an angle $-\theta_{inc}$. In the model we define two off-state parameters, combination of the LC indexes ordinary and extraordinary, n_o and n_e, together with the cell gap d. These parameters are $OPL = dn_o$ and $OPD = d\Delta n$, which correspond respectively to the magnitudes of the optical path length for the ordinary component and the optical path difference between extraordinary and ordinary components. Proper derivation leads to the following analytical expression for the retardance[11],

$$\Gamma = \frac{2\pi}{\lambda}\frac{OPL}{\cos\theta_{LC}}\left[\frac{1+(OPD/OPL)}{1+(OPD/OPL)\cos^2\varphi}-1\right] \tag{1}$$

According to Fig. 1, angle φ is given by,

$$\varphi(\theta_{inc},V) = \frac{\pi}{2} + \alpha(V) \mp \theta_{LC}(\theta_{inc}) \tag{2}$$

, where the minus (plus) sign applies for the forward (backward) passage. The total retardance in the PA-LCoS is given by the addition of the forward and backward retardances. In the case of normal incidence and LC director axis parallel to the entrance face, then Eq. (1) simplifies into the well-known expression $\Gamma = 2\pi d\Delta n/\lambda$. Our model produces a much

simpler expression and reduces the number of parameters when compared with the exact expressions for a homogeneous uniaxial anisotropic plate as we demonstrated[11] with experimental measurements.

2.2 Virtual PA-LC cell

To evaluate the physical significance of the three parameters in the model we consider the nematic LC E7 at room temperature (20ºC) and a cell gap of 2 μm. The LC mixture E7 is one of the classical compounds found in the literature dealing with LC devices[17]. We apply a sine-like tilt angle profile, which is a valid approximation as long as the applied voltages are small enough not to produce a saturation in the tilt angle. In many situations, availability of analytical expressions is a very interesting situation since parameters are then easier to be analysed to obtain the necessary in-depth physical insight. In the case of tilt angle profiles there is also an interest in obtaining analytic expressions for the tilt angle profiles as done by Abdulhalim and Menashe[13]. In the sine profile, the tilt angle α across the cell thickness z varies as,

$$\alpha = \alpha_{\max} \sin(\pi z / d) \tag{3}$$

, where d is the cell gap, and $\alpha_{\max}$ is the maximum tilt angle, which occurs in the midlayer of the cell. In Fig. 2 we show the sine-like tilt profile for various $\alpha_{\max}$ values. We consider the normalized thickness parameter $z' = z/d$ in the X-axis. We consider $\alpha_{\max}$ values in the interval from 0 to 70º since, as we will see in next Section, when fitting the on-state parameter $\alpha(V)$ we obtain that its values are within the range found already in commercial devices[11].

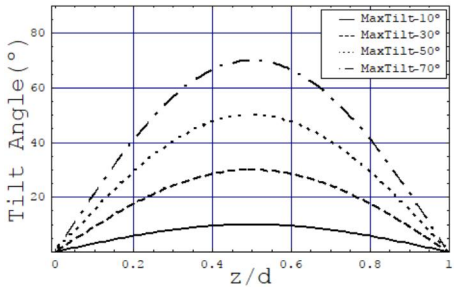

Figure 2. LC director sine-like tilt angle profiles across the thickness of the cell and for various $\alpha_{\max}$ values (in the legend).

As refractive indices we use the tabulated values provided in the paper by Li et al.[17] and interpolate them using the Cauchy relation to produce additional values at other wavelengths. In Table 1 we show the values for the ordinary and the extraordinary refractive index at wavelengths 633, 532 and 473 nm, which are the ones selected to compare with the results provided by the simplified model. Indeed the retardance is calculated for a total of 18 different equidistant wavelengths running from 473 to 634 nm across the whole visible spectrum.

Table 1. Values for the refractive indices for the three wavelengths specifically analysed in the paper.

λ (nm)	n_e	n_o
633	1.7371	1.5189
532	1.7646	1.5289
473	1.7935	1.5384

Once we generate the LC director profiles, then we apply the SF-FDTD to simulate the propagation of the incident electromagnetic field across the PA-LC cell. We consider the LC cell composed of the LC layer with a perfectly conducting mirror at the rear surface. The glass window at the entrance is not considered. This has only a residual impact in the degree of realism of the simulation and has the benefit of reducing significantly the number of points, thus the

memory resources needed, sampling the cell structure: the LC layer is 2 µm thick, whereas the glass window is typically a few millimeters thick, thus needing many more points in the sampling grid. To the entrance interface air-LC layer we add an antireflection (AR) thin film structure for the visible spectrum[18], mimicking the usual AR coating found in PA-LCoS devices.

According to the experimental method we use, the time-average Stokes polarimetric technique[11], we illuminate with light linearly polarized at 45º with respect to the director axis of the LC layer at the entrance face. The SF-FDTD provides the values for the electric field at the output of the reflective PA-LC cell. This enables to calculate the phase-shift between the electric field component polarized along the LC-director axis and the one orthogonally polarized. This phase-shift is the retardance of the PA-LC cell. In Fig. 3 (a), (b) and (c) we show the retardances as a function of $\alpha_{\max}$ calculated using the SF-FDTD approach for the virtual PA-LC and for the three wavelengths 633, 532 and 473 nm respectively. In the SF-FDTD calculations we consider angles of incidence at 0º (normal incidence), 3º, 25º, 35º and 45º, which cover a wide range of working conditions found in applications[19][20]. In Fig. 3, we represent angles 3º, 25º, 35º and 45º (see legend) since results at 0º and at 3º are almost equal. We clearly appreciate the non-linear monotonous decrease of retardance with $\alpha_{\max}$. We also verify that the retardance dynamic range becomes shorter for larger angles of incidence, which was also found in the experimental measurements in previous papers[19][20].

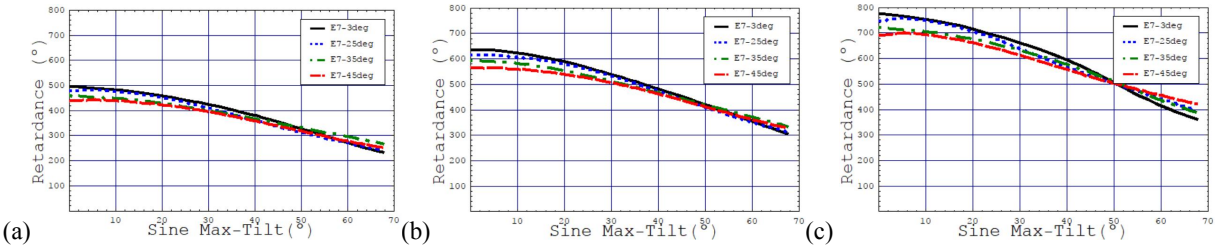

Figure 3. Retardance SF-FDTD simulated measurements for the various incidence angles (in the legend) and for the wavelengths: (a) 633 nm, (b) 532 nm, and (c) 473 nm.

We also produce by simulation the values for the off-state, i.e. when no voltage is applied to the device. To this goal we directly consider the results produced by the homogeneous uniaxial anisotropic slab expressions[21]: in the off-state the LC device has a uniform LC director distribution and the exact expression can be used with a higher accuracy. In Table 2 we show the retardance for the 5 angles of incidence and for the three wavelengths for the off-state.

Table 2. Values for the retardance in the off-state.

λ (nm)	Incidence angle (deg)				
	0	3	25	35	45
633	496.4	496.1	476.8	459.6	439.3
532	638.0	637.6	613.1	591.4	565.7
473	776.6	776.2	746.7	720.6	689.7

3. NUMERICAL RESULTS

To obtain the parameters in the model we fit the analytical expression to the simulated experimental results, which are generated with the SF-FDTD technique and the virtual PA-LC cell. In a first step we fit the off-state parameters, OPD and OPL, using the off-state retardance values in Table 2. These off-state parameters are wavelength dependent but do not depend on the angle of incidence. Afterwards, we fit the tilt angle, which depends on the applied voltage. We use the measurements taken at 3º and 35º for calibration of the model parameters, and the other two measurements, at 25º and 45º, to validate and analyse its predictive capability.

To serve as a reference, in Table 3 we give the true values for OPD and OPL calculated according to the refractive indices and cell gap value from Table 1. The fitted values obtained for OPD and OPL are given in Table 4. The figure of merit χ^2 to be minimized combines two squared differences: on one hand between theoretical and simulated retardance values normalized by the simulated value, and on the other hand between the theoretical and simulated ratios of the retardance values for the pair of incidence angles considered (3º and 35º) normalized by the simulated ratio. These two normalized squared differences are added up for the three wavelengths. This minimized value for χ^2 is given for each set of fitted parameters in Table 4 (2nd row). We want to remark that the theoretical expressions are nonlinear and to start the iterative optimization process we have to assign initial values to the parameters OPD and OPL. As we already demonstrated[11] our model provides the same resulting OPD and OPL values for a very wide range of starting values, thus not showing multiple, i.e. ambiguous, solutions. Then, in the third row we show the mean square error difference (MSE), which serves to validate the goodness of the agreement between theory and experiment for the on-state fitting of the tilt angle $\alpha(V)$ parameter. The figure of merit MSE is given by the square difference at each voltage between the theoretical and simulated retardance values normalized by the simulated value, added up for the whole range of voltages and for both incidences at 3º and 35º, and then divided by the total number of samples to produce a mean value. The on-state results will be later shown in the figures.

Table 3. Values for the OPD and OPL parameters calculated from the cell gap and the indices of refraction in Table 1.

λ (nm)	633	532	473
OPD(μm)	0.4364	0.4714	0.5102
OPL(μm)	3.0378	3.0578	3.0768

Table 4. OPD and OPL values obtained from the fitting procedure and for different values for n_{LC}. Figures of merit for the off-state χ^2 and for the on-state MSE comparison between theoretical and experimental results in 2nd and 3rd rows

n_{LC}	1.50	1.59	1.60	1.61	1.62	1.65	1.70
χ^2 Off-State	$4.8\text{x}10^{-5}$	$1.8\text{x}10^{-24}$	$7.1\text{x}10^{-28}$	$2.2\text{x}10^{-18}$	$2.8\text{x}10^{-20}$	$3.7\text{x}10^{-26}$	$2.5\text{x}10^{-20}$
MSE On-State	0.00050	0.00059	0.00060	0.00060	0.00060	0.00061	0.00063
	(μm)	(μm)	(μm)	(μm)	(μm)	(μm)	(μm)
OPD(633 nm)	0.4369	0.4364	0.4364	0.4364	0.4364	0.4364	0.4364
OPL(633 nm)	$24.02\text{x}10^{6}$	7.8298	6.8456	6.0775	5.4614	4.1772	2.9829
OPD(532 nm)	0.4722	0.4714	0.4714	0.4714	0.4714	0.4714	0.4714
OPL(532 nm)	$39.89\text{x}10^{6}$	9.9576	8.5336	7.4609	6.6237	4.9421	3.4506
OPD(473 nm)	0.5113	0.5102	0.5102	0.5102	0.5102	0.5102	0.5102
OPL(473 nm)	$49.53\text{x}10^{6}$	12.9004	10.7767	9.2462	8.0910	5.8679	3.9977

In Table 4 we show the results obtained for OPD and OPL for the three wavelengths and for different values of n_{LC} (first row). We show n_{LC} values ranging from 1.5 to 1.7, which fall within the typical range of values for liquid crystals. Specifically if we take into account the refractive indices for E7 in Table 1, the average refractive index, calculated as $(n_e + 2n_o)/3$, is 1.59, 1.61 and 1.62 respectively for the wavelengths 633, 532 and 473 nm. The average of the three values is 1.61.

In Table 4, the best MSE is obtained for $n_{LC} = 1.50$, where we actually obtain clearly a worse χ^2. This may seem contradictory but if we look at the MSE values, we see that they are very close to each other through the whole range of n_{LC} simulated. If we take a look at the OPD values for the three wavelengths, we see that they are similar to the four decimal number with respect to the ones shown in Table 3, except for $n_{LC} = 1.50$ where it is similar to the third decimal number, which is still a very good agreement. Values for OPL show a larger range of variation and we also observe that they do not coincide with the values in Table 3. Then, we can assure that OPD is actually a physically meaningful parameter whose value can be obtained with the technique proposed, which is robust to the value considered for n_{LC}.

Now, we fix the values for OPD and OPL in Eq. (1) and fit the tilt angle $\alpha(V)$, in Eq. (2). In this work, the role played by the voltage is actually expressed as a function of the maximum tilt angle $\alpha_{\max}$. Then the fitting procedure provides the relation $\alpha(\alpha_{\max})$. To apply the expression in Eq. (1) we consider the off-state solution in Table 4 for OPD and OPL obtained when $n_{LC} = 1.60$, where χ^2 in Table 4 showed the lowest value. The same figure of merit function χ^2 is now used for the on-state fitting procedure, and the optimization is run independently for each of the $\alpha_{\max}$ values. As experimental retardance we consider the FDTD values for incidence angles at 3º and 35º. In Fig. 4 (a) and (b) we show the retardance versus voltage plots for the theoretical fitting using the model (continuous line) and the experimental-FDTD data (dots) respectively for the incidence angles at 3º and 35º, and for the three wavelengths. We note that theoretical and FDTD results agree very well with each other at both incidences and for the three wavelengths.

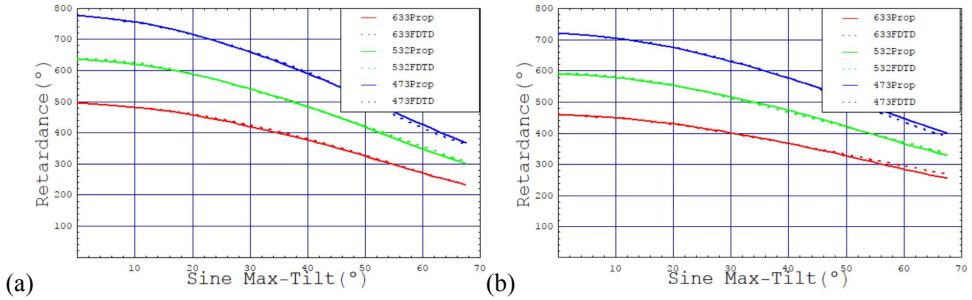

Figure 4. FDTD-experiment (dots) and theoretical fitting with the model (continuous line) for the wavelengths 633, 532 and 473 nm and for incidence at: (a) 3º; (b) 35º.

In Fig. 5 we show the fitted equivalent tilt angle in the model versus $\alpha_{\max}$, labeled as "Proposed Model". We also show the "Average Tilt" corresponding to the mean tilt value across the cell gap for the sine-like tilt profiles, shown in Fig. 2. We see that the "Average Tilt" follows a linear line, and the "Proposed Tilt" runs in parallel most of the range with a value about 4º larger. We might think of the "Proposed Model" tilt angle as a corrected average tilt able to provide correct values for the retardance of the non-homogeneous profiles. We note that we have limited our attention to a maximum $\alpha_{\max}$ of about 70º: within this range the fitted equivalent tilt angle runs from 0º to about 45º, which is within the range we found for commercial PA-LCoS microdisplays[11].

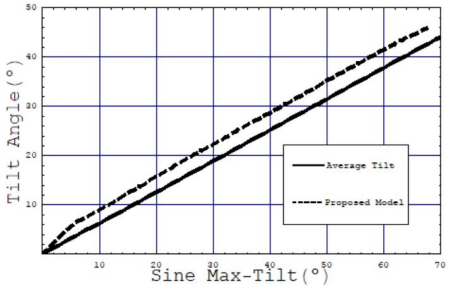

Figure 5. Fitted equivalent tilt angle as a function of $\alpha_{\max}$ for the sine profile.

Now, using the fitted tilt angle in Fig. 5 we test the predictive capability of the model at two other angles of incidence not used in the calibration. In Fig. 6 (a) and (b), respectively for incidence at 25º and 45º, we show both the theoretical values calculated with the model (continuous line) and the FDTD-experimental values (dots). Retardance is plotted as a function of the model-fitted tilt angle instead of $\alpha_{\max}$. We note the good agreement between model and FDTD-

experiment. We show quantitative evaluation of the predictive capability shown in Fig. 7 (a) and (b) respectively for angles of incidence 25º and 45º, where we provide the normalized retardance difference (theoretical minus FDTD-experimental retardance normalized by the theoretical values). The model proposed predicts the retardance with relative uncertainties that in most of the tilt angle range is less than 5%. In general, uncertainty increases with the increase in α_{max}. These results agree with the previous from experimental retardance measurements[11].

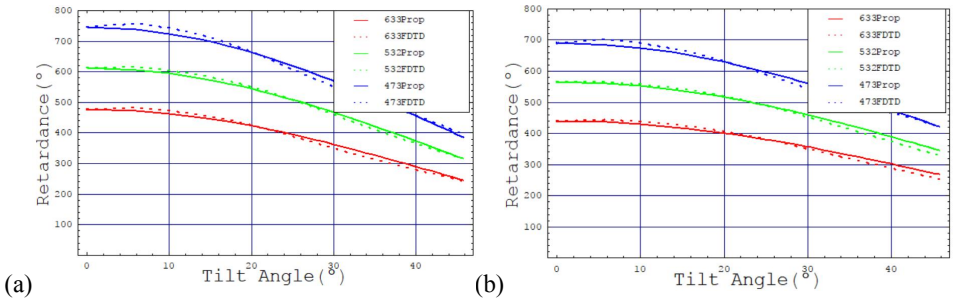

Figure 6. FDTD-experiment (dots) and prediction with the model (continuous line) for the wavelengths 633, 532 and 473 nm and for incidence at: (a) 25º; (b) 45º.

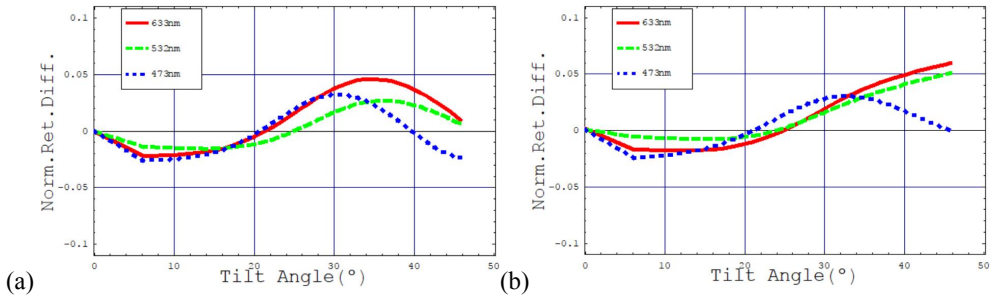

Figure 7. Difference between predicted and FDTD-experimental retardance normalized by the predicted value for wavelengths 633, 532 and 473 nm and for incidence at: (a) 25º, and (b) 45º.

4. CONCLUSIONS

We have analysed the physical relevance of the parameters of a simplified reverse-engineering model for PA-LC devices. Since manufacturers do not provide the values for the parameters of commercial devices, we have simulated a virtual PA-LC cell and the retardance values have been calculated by applying an efficient SF-FDTD technique. SF-FDTD is a rigorous electromagnetic approach providing realistic results. As tilt angle profile across the thickness of the cell we have assumed a sine-like shape. As long as applied voltages are not large enough to produce tilt angles close to 90º, i.e. tilt saturation, this is a reasonable approximation. Furthermore, from previous experimental measurements, we learn that this is within the dynamic range of tilt angles in commercial PA-LCoS microdisplays, thus the sine-like approximation becomes a good option. The liquid crystal considered for the virtual PA-LC cell is the E7 compound and the cell thickness is 2 µm.

In the application of our simplified model we have obtained that two of the three parameters, the OPD and the tilt angle, provide physically relevant values, thus the model can be used as a means to inspect some internal physical properties of the cell. In addition, we have also verified under this highly controlled environment with our virtual PA-LC cell, that its predictive capability is very high, with relative uncertainties lower than 5% in the calculation of the retardance across the whole visible spectrum and for a wide range of incidence angles from 0 to 45º. Then, the model is very versatile and easy

to apply, what makes it very useful to characterize the possibilities of PA-LC devices in novel applications such as in experiments dealing with unconventional polarization states[22][23] or in spectrum modulation[24].

ACKNOWLEDGEMENTS

Work supported by Ministerio de Economía, Industria y Competitividad (Spain) (FIS2014-56100-C2-1-P and FIS2015-66570-P) and by Generalitat Valenciana (Spain) (PROMETEO II/2015/015).

REFERENCES

[1] S. T. Wu and D. K. Yang, [Reflective Liquid Crystal Displays], John Wiley & Sons Inc. (2005).
[2] G. Lazarev, A. Hermerschmidt, S. Krüger, and S. Osten, "LCOS Spatial Light Modulators: Trends and Applications," in [Optical Imaging and Metrology: Advanced Technologies], W. Osten and N. Reingand, eds., John Wiley & Sons (2012).
[3] N. Collings, T. Davey, J. Christmas, D. Chu, and B. Crossland, "The Applications and Technology of Phase-Only Liquid Crystal on Silicon Devices," J. Display Technol. 7, 112-119 (2011).
[4] Z. Zhang, Z. You, D. Chu, "Fundamentals of phase-only liquid crystal on silicon (LCOS) devices," Light: Science & Applications 3, 1-10 (2014).
[5] F.J. Martínez, A. Márquez, S. Gallego, J. Francés, I. Pascual, and A. Beléndez, "Retardance and flicker modeling and characterization of electro-optic linear retarders by averaged Stokes polarimetry," Opt. Lett. 39, 1011-1014 (2014).
[6] F. J. Martínez, A. Márquez, S. Gallego, M. Ortuño, J. Francés, A. Beléndez, and I. Pascual, "Electrical dependencies of optical modulation capabilities in digitally addressed parallel aligned LCoS devices," Opt. Eng. 53, 067104 (2014).
[7] F.J. Martínez, R. Fernández, A. Márquez, S. Gallego, M. L. Álvarez, I. Pascual, and A. Beléndez. "Exploring binary and ternary modulations on a PA-LCoS device for holographic data storage in a PVA/AA photopolymer," Opt. Express 23, 20459-20479 (2015).
[8] A. Hermerschmidt, S. Osten, S. Krüger, and Thomas Blümel, "Wave front generation using a phase-only modulating liquid-crystalbased micro-display with HDTV resolution, " Proc. SPIE 6584, 65840E (2007).
[9] A. Lizana, I. Moreno, A. Márquez, E. Also, C. Iemmi, J. Campos, and M.J. Yzuel, "Influence of the temporal fluctuations phenomena on the ECB LCoS performance," Proc. SPIE 7442, 74420G-1 (2009).
[10] J. García-Márquez, V. López, A. González-Vega, E. Noé, "Flicker minimization in an LCoS spatial light Modulator," Opt. Express 20, 8431-8441 (2012).
[11] F. J. Martínez, A. Márquez, S. Gallego, J. Francés, I. Pascual, A. Beléndez, "Effective angular and wavelength modelling of parallel aligned liquid crystal devices," Opt. Lasers Eng. 74, 114-121 (2015).
[12] P. Yeh, C. Gu, [Optics of Liquid Crystal Displays], John Wiley & Sons Inc. (1999).
[13] I. Abdulhalim, D. Menashe, "Approximate analytic solutions for the director profile of homogeneously aligned nematic liquid crystals," Liquid Crystals 37, 233-239 (2010).
[14] A. Taflove, S. C. Hagness, [Computational Electrodynamics: The Finite-Difference Time-Domain Method, 2nd ed.], Artech House (2000).
[15] C. Oh, M. J. Scuti, "Time-domain analysis of periodic anisotropic media at oblique incidence: an efficient FDTD implementation," Opt. Express 14, 11870–11884 (2006).
[16] J. Francés, S. Bleda, M. L. Lázara, F. J. Martínez, A. Márquez, C. Neipp, A. Beléndez, "Acceleration of split-field finite difference time-domain method for anisotropic media by means of graphics processing unit computing," Opt. Eng. 53, 011005-1/10 (2014).
[17] J. Li, C-H. Wen, S. Gauza, R. Lu, S-T. Wu, "Refractive Indices of Liquid Crystals for Display Applications," J. Disp. Technol. 1, 51-61 (2005).
[18] F. Abeles, [Optics of Thin Films in Advanced Optical Techniques], North-Holland Publishing Co. (1967).
[19] A. Lizana, N. Martin, M. Estapé, E. Fernández, I. Moreno, A. Márquez, C. Iemmi, J. Campos, M. J. Yzuel, "Influence of the incident angle in the performance of Liquid Crystal on Silicon displays," Opt. Express 17, 8491-8505 (2009).

[20] F.J. Martínez, A. Márquez, S. Gallego, M. Ortuño, J. Francés, A. Beléndez, and I. Pascual, "Averaged Stokes polarimetry applied to evaluate retardance and flicker in PA-LCoS devices," Opt. Express 22, 15064-15074 (2014).
[21] A. Lien, "Extended Jones matrix representation for the twisted nematic liquid-crystal display at oblique incidence," Appl. Phys. Lett. 57, 2767-2769 (1990).
[22] T. G. Brown, Q. Zhan, "Focus Issue: Unconventional Polarization States of Light," Opt Express 18, 10775-10776 (2010).
[23] X. Zheng, A. Lizana, A. Peinado, C. Ramírez, J. L. Martínez, A. Márquez, I. Moreno, J. Campos, "Compact LCOS-SLM based polarization pattern beam generator," J. Lightwave Technol. 33, 2047-2055 (2015).
[24] I. Moreno, J. V. Carrión, J. L. Martínez, P. García-Martínez, M. M. Sánchez-López, J. Campos, "Optical retarder system with programmable spectral retardance," Opt. Lett. 39, 5483-5486 (2014).